Beyond the Paired t-Test: Equivalence-Based Validation of Centrifugal Stress Models for Solid, Tapered-Web, and Gaussian Flywheel Discs

Edrian Cliff D. del Pilar[1*], Deolinda E. Caparroso[1]

[1]Graduate School and College of Engineering, Cebu Technological University – Main Campus, M.J. Cuenco Ave. cor. R. Palma St., Cebu City 6000, Philippines

[*]Corresponding author

DOI: https://doi.org/10.51244/IJRSI.2026.1310000074

Received: 08 October 2026; Accepted: 13 October 2026; Published: 01 November 2026

ABSTRACT

Comparing the fatigue lives of competing flywheel shapes first requires trusted stress models. This study validates axisymmetric plane-stress models of three bore-less discs, each with a 0.2 m radius and a 25 mm rim: a constant-thickness solid disc in structural steel, a linearly tapered web (50 mm at the hub) in carbon steel, and a Gaussian profile (30.2 mm at the hub) in ASTM Class 30 cast iron. At 522.57 rad/s, each model was compared at 40 radial positions with its matching published solution and, independently, with a converged two-dimensional axisymmetric finite element analysis (FEA). Agreement was judged by the area-under-the-curve (AUC) difference, point-wise errors, the paired t-test, and the two one-sided tests (TOST) procedure with a ±5% equivalence margin, with confidence intervals corrected for serial correlation through an effective sample size and a moving-block bootstrap. All comparisons passed the 15% AUC limit (largest deviation 4.83%), yet the t-test misjudged two cases: it rejected the solid disc despite mean offsets of only −0.04 and +0.12 MPa, and accepted the tapered-web hoop stress ($p = 0.314$) although the curves differed by 11.92 MPa at the rim. Correlation-corrected TOST and a point-wise envelope check found the solid and Gaussian discs equivalent to their references and the tapered web not equivalent. The FEA agreed with all three models to within 1.2% of peak stress but differed from the tapered-web reference by up to 12.0 MPa, showing that the discrepancy comes from the reference's neglect of the thickness-gradient term. With all discs in the same steel, the tapered web had the highest energy shape factor (0.718, against 0.631 and 0.606). Validation should pair AUC with point-wise errors and a correlation-aware equivalence test, and should separate agreement with a reference from model accuracy.

Keywords: flywheel disc, centrifugal stress, model validation, area under the curve, equivalence testing

NOMENCLATURE

Symbol	Description	Symbol	Description
AUC	Area under the stress–radius curve (MPa·mm)	b	Outer radius of the disc (m)
CI	Confidence interval	d_i	Paired difference at point i, $\sigma_{current} - \sigma_{reference}$ (MPa)
FEA	Finite element analysis	h(r)	Axial thickness at radius r (mm)
LEFM	Linear elastic fracture mechanics	K	Energy shape factor (–)
RMSE	Root-mean-square error (MPa)	N	Number of matched points (–)
TOST	Two one-sided tests	r, R	Radial coordinate (m, mm)

ISSN No. 2321-2705 | DOI: 10.51244/IJRSI |Volume XIII Issue X October 2026

α	Significance level (–)	E	Young's modulus (GPa)
Δ_E	Equivalence margin (MPa)	ν, ρ	Poisson's ratio (–), density (kg/m^3)
μ_d	Population mean of paired differences (MPa)	ω	Angular velocity (rad/s)
N_{eff}	Effective sample size (–)	r_1	Lag-1 autocorrelation of d_i (–)
s_d	Standard deviation of paired differences (MPa)	σ_r, σ_θ	Radial and hoop (tangential) stress (MPa)

INTRODUCTION

A spinning flywheel is a simple way to hold energy: charge it by speeding it up, discharge it by letting it slow down. That simplicity, together with high power and long cycle life, explains why flywheels now appear in grid frequency control, braking-energy recovery in vehicles and trains, and backup power (Pullen, 2019; Li & Palazzolo, 2022; Xu et al., 2023). Composite rotors reach the highest energy densities, but for low- and medium-speed duty a metal rotor is usually the sensible choice: it is cheap, easy to make, and recyclable (Kale & Secanell, 2018). In a metal rotor, one design variable does most of the work. The shape of the cross-section sets the mass, the moment of inertia, and the stress field all at once (Kale et al., 2021).

What eventually limits such a rotor is usually fatigue rather than a single overload. A crack that grows over many speed cycles is especially dangerous in a flywheel, because the stored energy is released in one event when the rim finally lets go. Studies of grid-connected and transport flywheels have shown that safe crack sizes and critical locations cannot be read from peak-stress margins alone; they have to come from fracture mechanics (Wang et al., 2002; Rouse et al., 2021). Linear elastic fracture mechanics (LEFM) and the Paris crack-growth law supply the theory (Paris et al., 1961; Anderson, 2017), and three-dimensional finite element analysis (FEA) now makes crack-growth simulation routine (Alshoaibi & Fageehi, 2024). Nuñez et al. (2025), for instance, combined a validated FEA model of a steel flywheel with a Gaussian-process surrogate for the energy release rate and traced mixed-mode crack growth through the rotor.

All of that work stands on the stress field. Crack-initiation sites are picked from it, fatigue amplitudes come from it, and stress intensity factors are driven by it. Designers have long reshaped the rotor profile to control this field. Stodola's (1927) constant-stress disc and the exponential and Gaussian discs solved by Eraslan and Orcan (2002) and Eraslan (2005) thin the section towards the rim. Conical and tapered-web discs do the same with a straight taper (Garcia et al., 2025; Arun et al., 2026). Shape-optimisation studies confirm that such changes shift both energy density and stress (Berger & Porat, 1988; Kale et al., 2021; Coppedé et al., 2024). What is still missing is a side-by-side comparison of several shapes inside one stress, fatigue, and fracture framework. Before that comparison is worth anything, though, each shape's stress model needs to be shown to be right.

In flywheel papers, that demonstration is usually an area-under-the-curve (AUC) comparison with a published stress plot, backed by a paired t-test on point values. Nuñez et al. (2025) accepted an AUC deviation under 15% and a t-test with $p = 0.2575$ as proof of fidelity. Both steps have a blind spot. An integral lets errors of opposite sign along the radius cancel out. The t-test answers the question "is the average difference exactly zero?", which is not what an engineer validating a model wants to know. A large p-value only says that a difference was not detected; it does not say that the difference is small. Conversely, a tiny but very steady offset can look highly significant (Schuirmann, 1987; Lakens, 2017). On top of this, stresses read off one smooth curve are neither independent nor normally distributed, so the test's own assumptions do not hold.

This paper is the first stage of a larger comparison of fatigue life and crack growth in three flywheel shapes: a solid disc, a tapered web, and a Gaussian disc. Its scope is the stress models alone; no fatigue or fracture results are reported here. We make four contributions. First, we build the three plane-stress models and check them against an independent axisymmetric finite element analysis that does not rely on the plane-stress assumption. Second, we test each model against the published solution that matches its geometry, using the AUC comparison, point-wise errors, and the paired t-test. Third, we show that equivalence testing with the two one-sided tests (TOST) procedure, corrected for the serial correlation of points taken along one curve, settles the cases where those measures disagree, and we justify the equivalence margin from the intended use of the stresses. Fourth, we separate two questions that are often merged: whether a model agrees with a given reference, and whether the model is accurate. We also report a speed-independent energy measure for the three shapes, including a same-material comparison, since that is the quantity a designer will later weigh against fatigue resistance.

METHODOLOGY

Research design and workflow

The study is a comparative computational one. Disc geometry is the variable we change; radial and hoop stress along the radius are what we measure. No single source covers all three shapes, so each model was paired with the reference that shares its geometry. Figure 1 sets out the two stages: building the models, then validating them statistically. Because agreement with a published solution does not by itself prove that a model is accurate, every model was also compared with an independent axisymmetric finite element analysis (FEA). The stress fields will later feed the three-dimensional fatigue and crack-growth analyses of the wider study, which are outside the scope of this paper.

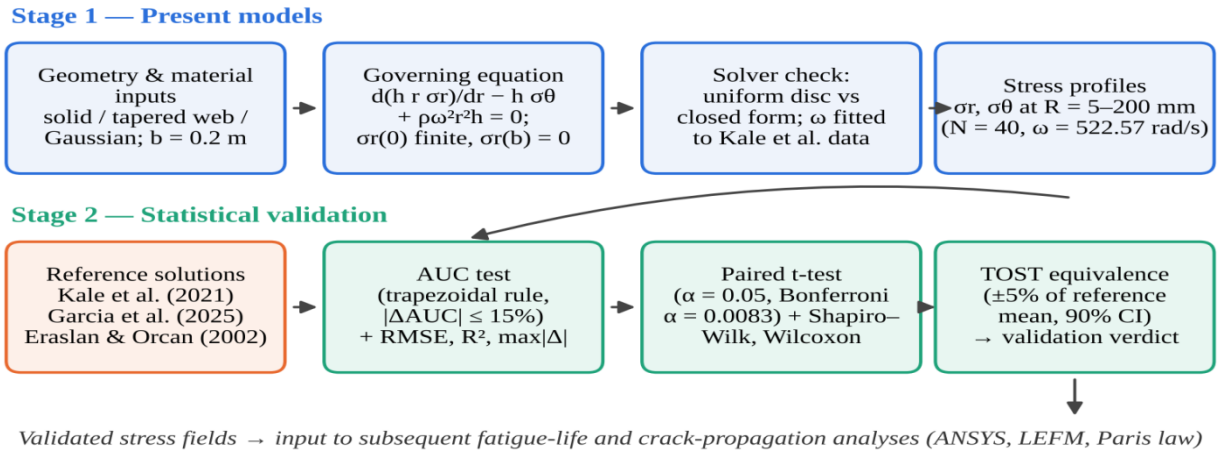


Figure 1. Model development and statistical validation workflow

Flywheel geometries and materials

All three discs are solid (no bore), with an outer radius b = 0.2 m and a 25 mm rim (Figure 2). The solid disc is 25 mm thick throughout. The tapered web falls linearly from 50 mm at the centre to 25 mm at the rim, a 2:1 ratio. The Gaussian disc follows $h(r) = 30.2 \exp(-4.724r^2)$ mm with r in metres; its 30.2 mm centre thickness came from the constant-stress (de Laval) relation, anchored to the 25 mm rim. Materials follow common industrial practice for each form: structural steel for the solid disc, carbon steel for the tapered web, and ASTM Class 30 grey cast iron for the Gaussian disc. Table 1 lists the inputs together with the mass, kinetic energy, and shape factor of each disc. Because the materials differ, the energy comparison is repeated with all three discs in structural steel, so that the effect of shape can be separated from that of material (Table 6).

ISSN No. 2321-2705 | DOI: 10.51244/IJRSI |Volume XIII Issue X October 2026

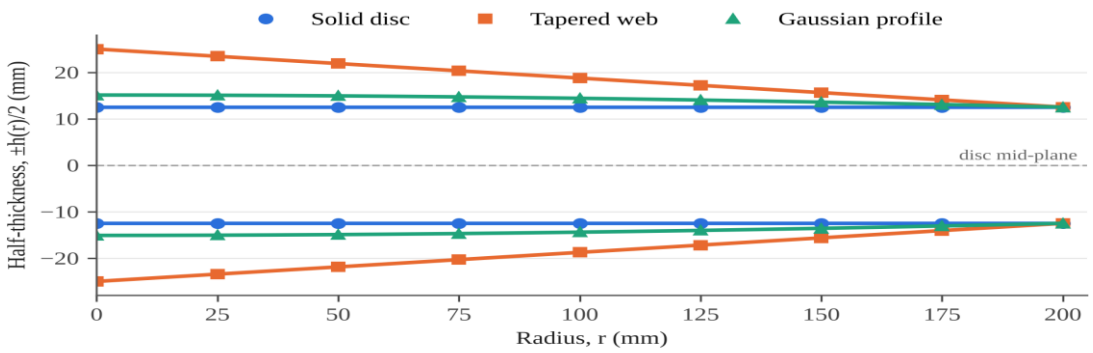


Figure 2. Axial half-sections of the three flywheel discs (outer radius b = 200 mm)

Table 1. Disc inputs, mass properties, and reference solutions

Design	Material	E (GPa)	ν	ρ (kg/m³)	Thickness h(r)	Mass (kg)	KE at ω (kJ)	K	Reference
Solid disc	Structural steel	210	0.3	7,850	25 mm, constant	24.66	67.3	0.606	Kale et al. (2021)
Tapered web	Carbon steel	210	0.3	7,850	Linear, 50 → 25 mm	32.88	80.8	0.718	Garcia et al. (2025)
Gaussian disc	Cast iron ASTM-30	101	0.23	7,510	30.2 exp(−4.724r²) mm	25.97	68.7	0.643	Eraslan & Orcan (2002)

$KE = \frac{1}{2}I\omega^2$ at ω = 522.57 rad/s, from integrating each thickness profile. $K = KE\cdot\rho/(m\cdot\sigma_{max})$ is the energy shape factor; it does not depend on speed because KE and σ_{max} both scale with ω^2.

Governing equations and operating condition

For a thin disc of varying thickness h(r) under axisymmetric plane stress, radial equilibrium reads (Timoshenko & Goodier, 1970)

$$d(h\cdot r\cdot\sigma_r)/dr - h\cdot\sigma_\theta + \rho\omega^2 r^2 h = 0 \qquad (1)$$

We wrote Eq. (1) in terms of radial displacement, using the plane-stress Hooke relations, and solved it as a two-point boundary-value problem: the stress stays finite at the centre, and the rim is free, $\sigma_r(b) = 0$. For a disc of constant thickness the problem has the familiar closed-form answer

$$\sigma_r = (3+\nu)\rho\omega^2(b^2 - r^2)/8, \quad \sigma_\theta = \rho\omega^2[(3+\nu)b^2 - (1+3\nu)r^2]/8 \qquad (2)$$

and the solver matched it exactly. As a second, independent check, the three profiles were re-solved with a collocation boundary-value routine; it agreed with the model stresses at every one of the 40 comparison points to within 2×10^{-4} MPa. To make sure the model and the Kale et al. (2021) benchmark carry the same load, we fitted Eq. (2) to the benchmark by least squares. The fit returned ω = 522.57 rad/s (about 4,990 rpm) and ν = 0.30, the value the benchmark assumes. All three discs were then run at that speed. One consequence is worth stating: in a single-material disc the elastic modulus cancels out of the stresses, so the structural-steel and carbon-steel assignments give identical results for identical shapes, and cast iron changes the answer only through its lower density and Poisson's ratio.

Reference solutions

Table 2 summarises the comparison basis. The solid disc is checked against the radial and hoop stresses tabulated by Kale et al. (2021), the same benchmark Nuñez et al. (2025) used. The tapered web is checked against the closed-form stress function for conical flywheels by Garcia et al. (2025). The Gaussian disc is checked against the exponential-thickness solution of Eraslan and Orcan (2002), which is written with the

ISSN No. 2321-2705 | DOI: 10.51244/IJRSI |Volume XIII Issue X October 2026

Kummer confluent hypergeometric function (Eraslan, 2005). Garcia et al. (2025) obtain their closed form by neglecting the term (r/t)(dt/dr) in the equilibrium equation, an approximation intended for gentle tapers; its consequences for the 2:1 taper studied here are examined in the results.

Table 2. Reference solutions used for comparison

Design	Reference	Solution used
Solid disc	Kale et al. (2021); Timoshenko & Goodier (1970)	Published radial and hoop stresses; Eq. (2) used to recover ω.
Tapered web	Garcia et al. (2025)	Thickness $t = A + Br$; stress function $F = c_0 r - (3 + \nu)\rho\omega^2 r^3(A/8 + Br/15)$; $\sigma_r = F/(t \cdot r)$, $\sigma_\theta = F'/t + \rho\omega^2 r^2$; for a solid disc $c_1 = 0$ and $F(b) = 0$. The term (r/t)(dt/dr) is dropped.
Gaussian disc	Eraslan & Orcan (2002); Eraslan (2005); Stodola (1927)	$h = h_0 \exp[-n(r/b)^k]$, $k = 2$: $\sigma_r = S\{1 - e^{\beta(r^2-b^2)} \cdot M(a,2,-\beta r^2)/M(a,2,-\beta b^2)\}$, $S = \rho\omega^2/(2\beta)$, $a = (1 - \nu)/2$, M = Kummer function; σ_θ follows from Eq. (1).

Independent finite element verification

The Gaussian model and its reference solve the same equation, and the tapered-web reference is approximate, so agreement with the references cannot by itself establish that the models are accurate. Each disc was therefore also analysed with a two-dimensional axisymmetric FEA written by the authors in Python (NumPy and SciPy). Unlike the plane-stress model, the FEA represents the actual half-section, $0 \le z \le h(r)/2$, and solves the full axisymmetric elasticity equations, including axial and shear strain, under the centrifugal body force $\rho\omega^2 r$. Nine-node Lagrangian quadrilaterals with 3 × 3 Gauss integration were used on a mapped mesh, with $u_r = 0$ on the axis, $u_z = 0$ on the mid-plane by symmetry, and all other surfaces free of traction.

Thickness-averaged radial and hoop stresses were extracted at the 40 comparison radii, because the plane-stress solution represents the average through the thickness. Refining the mesh from 40 × 4 to 160 × 16 elements (radial × axial) changed the peak stress of every disc by less than 0.1%, and the 160 × 16 results are reported. For the solid disc the FEA reproduced the closed-form solution of Eq. (2) to within 0.007 MPa. The FEA is a numerical check that is independent of both the plane-stress model and the published references; it is not a substitute for physical measurement.

Area under the curve comparison

Stresses were sampled every 5 mm from R = 5 to 200 mm, giving N = 40 pairs per comparison. The centre point was left out because the Kale et al. (2021) data stop short of it. Areas were found with the trapezoidal rule,

$$AUC = \Sigma \tfrac{1}{2}(\sigma_i + \sigma_{i+1})(R_{i+1} - R_i) \qquad (3)$$

and compared as a percentage of the reference area:

$$\Delta AUC\ (\%) = (AUC_{current} - AUC_{reference}) / AUC_{reference} \times 100 \qquad (4)$$

Following Nuñez et al. (2025), $|\Delta AUC| \le 15\%$ was retained as a screening limit so that the results remain comparable with that study; it is not used as the acceptance criterion. A tolerance on an integral cannot be tailored to a geometry in any useful way, because errors of opposite sign along the radius cancel whatever the disc shape. We therefore also report each case against a stricter 5% limit and base the decision on the point-wise and equivalence measures that follow. Three point-wise measures were added: the largest absolute difference $\max|d_i|$, the root-mean-square error, and the coefficient of determination,

$$RMSE = [\Sigma\, d_i^2 / N]^{1/2}, \quad R^2 = 1 - \Sigma\, d_i^2 / \Sigma\, (\sigma_{ref,i} - \bar{\sigma}_{ref})^2 \qquad (5)$$

with $d_i = \sigma_{current,i} - \sigma_{reference,i}$.

Paired t-test

Six two-tailed paired t-tests were run, one per disc and stress component. We kept them separate on purpose: each pairs a different shape and material with a different reference, so pooling them would mix data that have nothing in common. With H_0: $\mu_d = 0$ against H_1: $\mu_d \neq 0$, the statistic is

$$t = \bar{d} / (s_d / \sqrt{N}), \quad df = N - 1 = 39 \qquad (6)$$

where $\bar{d}$ and s_d are the mean and standard deviation of the differences. Decisions are given at $\alpha = 0.05$ and, to allow for six tests, at the Bonferroni level $0.05/6 = 0.0083$ (Dunn, 1961). Normality of the differences was checked with the Shapiro–Wilk test (Shapiro & Wilk, 1965), and the Wilcoxon signed-rank test (Wilcoxon, 1945) was run as a distribution-free cross-check. For each case we also plotted the difference against the pair mean (Bland & Altman, 1986), with the mean difference and its 95% limits.

Equivalence testing

Failing to find a difference is not the same as showing agreement, so we also asked the question the other way round: is the difference small enough to ignore? The TOST procedure answers this (Schuirmann, 1987; Lakens, 2017). Two one-sided nulls, $\mu_d \leq -\Delta_E$ and $\mu_d \geq +\Delta_E$, are both rejected at $\alpha = 0.05$, and equivalence follows, when the 90% confidence interval of the mean difference sits inside the margin:

$$-\Delta_E < \bar{d} - t_{0.05,39} \cdot s_d/\sqrt{N} \quad \text{and} \quad \bar{d} + t_{0.05,39} \cdot s_d/\sqrt{N} < +\Delta_E \qquad (7)$$

The margin was set at 5% of the mean reference stress, $\Delta_E = 0.05 \cdot \bar{\sigma}_{ref}$, from the intended use of the stresses rather than from statistical convention, since the accuracy a validation must demonstrate depends on what the model will be used for (American Society of Mechanical Engineers [ASME], 2019; Oberkampf & Roy, 2010). Three considerations support this value. First, centrifugal stress scales with ω^2, so a 5% stress error is equivalent to a speed error of only about 2.5%, which gives the margin a direct physical meaning for a designer. Second, the stresses will feed Paris-law crack-growth calculations, in which the growth rate scales with the stress range raised to an exponent m of about 3 for steels (Anderson, 2017); a 5% stress error therefore changes the predicted growth rate by about 16%, which is small compared with the scatter of measured crack-growth data. Third, 5% is a third of the AUC screening limit, so equivalence is the stricter test. Because the margin remains a judgement, the verdicts were also checked for margins from 1% to 10%, and the smallest margin at which each case would pass is reported.

Points read from one smooth curve are serially correlated, so the 40 differences carry less information than 40 independent observations, and $s_d/\sqrt{N}$ understates the uncertainty of the mean. Two corrections were applied. First, the interval in Eq. (7) was recomputed with the effective sample size $N_{eff} = N(1 - r_1)/(1 + r_1)$ in place of N, with $N_{eff} - 1$ degrees of freedom, where r_1 is the lag-1 autocorrelation of the differences (Bayley & Hammersley, 1946). Second, a moving-block bootstrap (Künsch, 1989), with blocks of eight consecutive points and 20,000 resamples, gave a distribution-free 90% interval that preserves the local correlation. Because any statistical test on deterministic curves remains an approximation, a deterministic envelope check was also applied: $\max|d_i| < \Delta_E$, which requires every point, not only the mean, to lie inside the margin.

A model was counted as agreeing with its reference only if it passed the AUC screen, the correlation-corrected TOST, and the envelope check for both stress components. Agreement with the FEA, which measures model accuracy rather than agreement with a particular reference, was judged by the same envelope check.

RESULTS AND DISCUSSION

Stress distributions and energy storage

Figures 3 and 4 overlay the model stresses (markers) on the reference curves (lines). At 522.57 rad/s the solid disc is the most heavily loaded, reaching 35.37 MPa at the centre, where radial and hoop stress coincide. The Gaussian disc brings the centre stress down to 30.89 MPa, about 13% lower; roughly half of this reduction comes from its shape and the rest from the lower density and Poisson's ratio of cast iron (Table 6). The tapered

ISSN No. 2321-2705 | DOI: 10.51244/IJRSI |Volume XIII Issue X October 2026

web does better still: its peak radial stress is 26.87 MPa at R = 30 mm and its peak hoop stress is 26.74 MPa at R = 40 mm, roughly 24% below the solid disc. Every value is far below the yield strength of the steels and the roughly 207 MPa tensile strength of Class 30 cast iron, which confirms that the linear elastic assumption holds at this speed.

Lower stress costs material. At the same speed the tapered web weighs 33% more than the solid disc and stores 20% more energy, yet 10% less per kilogram (2.46 against 2.73 kJ/kg). Comparing shapes at a fixed speed is a little unfair, however, because a lower-stressed disc could simply be spun faster. The shape factor K in Table 1 removes that bias: it measures the energy stored per unit mass when each disc is run up to the same peak stress. On that basis the ranking flips. The tapered web leads with K = 0.718, the Gaussian disc follows at 0.643, and the solid disc trails at 0.606, the textbook value for a flat disc. The tapered web therefore gives the most energy per kilogram for a given stress limit; whether that advantage survives fatigue and crack growth is left to the next stage of the study and is not claimed here.

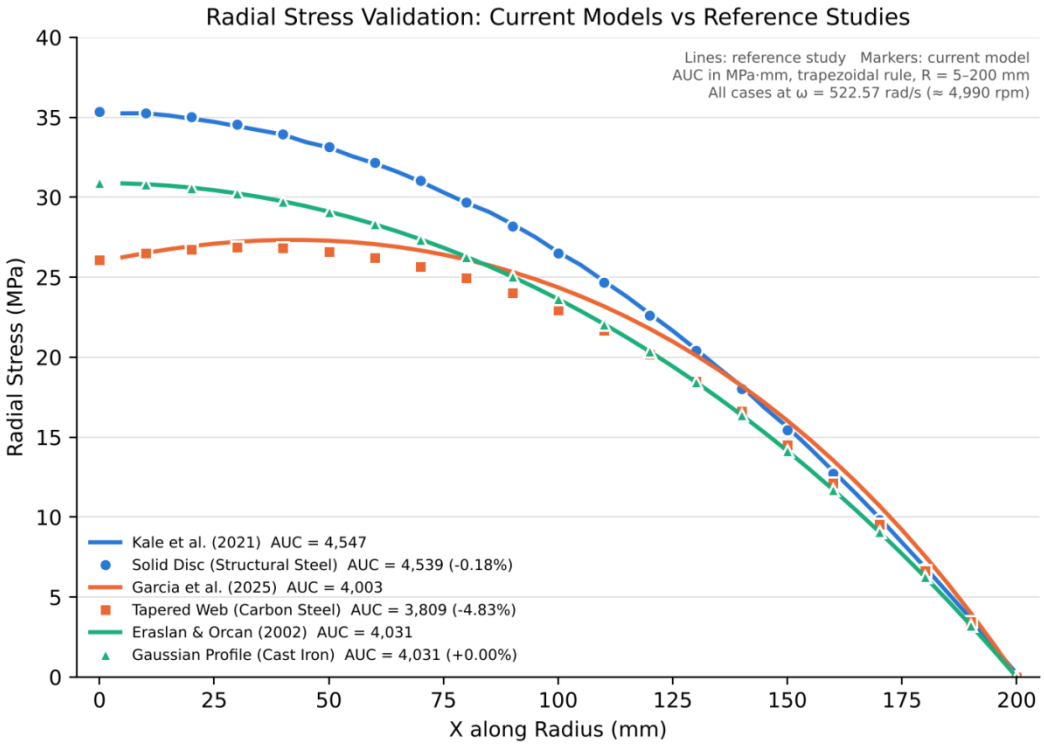


Figure 3. Radial stress: present models (markers) against reference solutions (lines), with AUC

ISSN No. 2321-2705 | DOI: 10.51244/IJRSI |Volume XIII Issue X October 2026

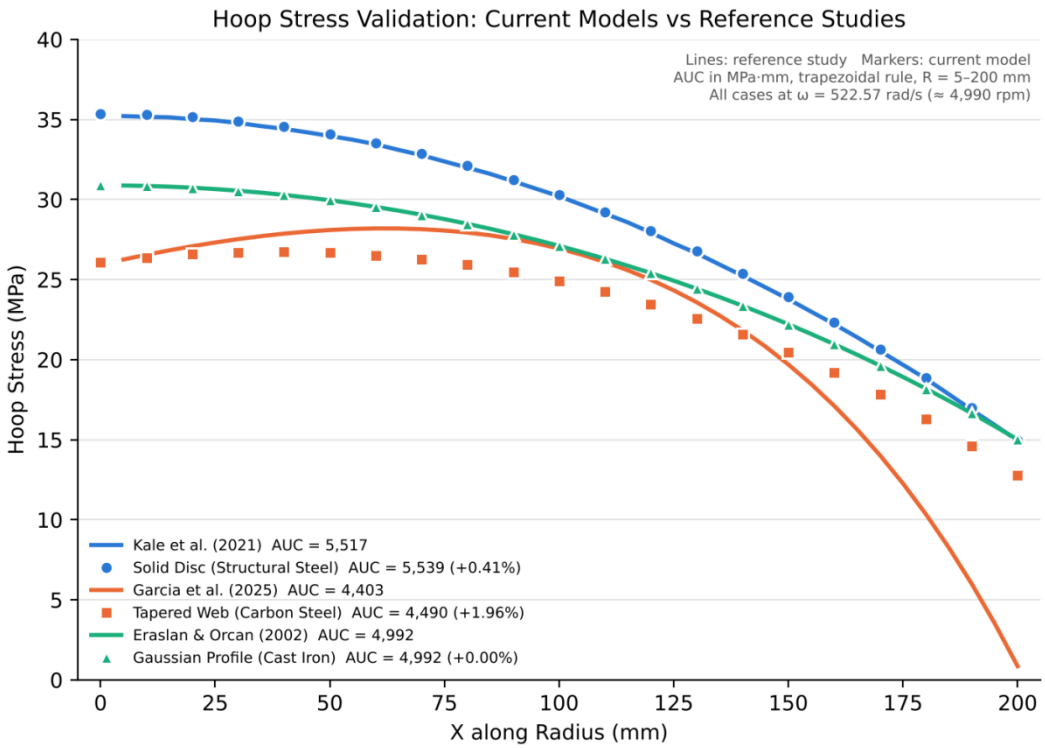


Figure 4. Hoop stress: present models (markers) against reference solutions (lines), with AUC

The materials were chosen to reflect how each form is usually made, but they blur the comparison of shapes. Table 6 therefore repeats the calculation with all three discs in structural steel. The elastic modulus does not

enter the stresses and K does not depend on density, so only the Gaussian disc changes. In steel its peak stress is 32.91 MPa, 7.0% below the solid disc against 24.0% for the tapered web, and its K falls slightly from 0.643 to 0.631 because of the higher Poisson's ratio. The ranking of the shapes on K is unchanged: tapered web, Gaussian disc, then solid disc.

Table 6. Effect of material: mass properties at ω = 522.57 rad/s with all discs in structural steel

Design	Material	Mass (kg)	KE (kJ)	Peak stress (MPa)	Reduction vs solid disc	K
Solid disc	Structural steel	24.66	67.3	35.37	–	0.606
Tapered web	Structural steel†	32.88	80.8	26.87	24.00%	0.718
Gaussian disc	Structural steel	27.15	71.8	32.91	7.00%	0.631
Gaussian disc	Cast iron ASTM-30 (as studied)	25.97	68.7	30.89	12.70%	0.643

†Carbon steel and structural steel share E, ν, and ρ in this study (Table 1), so the tapered-web results are identical for either. $K = KE \cdot \rho/(m \cdot \sigma_{max})$ is independent of density and speed.

Area under the curve

Table 3 collects the AUC results and point-wise errors. The solid disc sits within −0.18% (radial) and +0.41% (hoop) of Kale et al. (2021), with an RMSE near 0.12 MPa and R^2 of at least 0.9996. The Gaussian disc reproduces Eraslan and Orcan (2002) to four decimal places, so its differences round to 0.00%. The tapered web is off by −4.83% in radial stress and +1.96% in hoop stress against Garcia et al. (2025). All six comparisons clear the 15% limit. They would also clear a 5% limit, the largest deviation being 4.83%, so the choice of AUC

ISSN No. 2321-2705 | DOI: 10.51244/IJRSI |Volume XIII Issue X October 2026

tolerance affects no verdict in this study. More importantly, the tapered-web hoop case below shows an error that no AUC tolerance could detect.

Table 3. Area under the curve (MPa·mm) and point-wise errors, R = 5–200 mm

Stress	Design	AUC reference	AUC current	ΔAUC	Max |d| (MPa)	RMSE (MPa)	R^2
Radial	Solid disc	4,546.88	4,538.54	−0.18%	0.2159	0.1163	0.9999
Radial	Tapered web	4,002.79	3,809.32	−4.83%	1.6074	1.1041	0.9812
Radial	Gaussian disc	4,030.86	4,030.86	0.00%	0	0	1
Hoop	Solid disc	5,516.51	5,539.21	0.41%	0.1606	0.119	0.9996
Hoop	Tapered web	4,403.43	4,489.92	1.96%	**11.9164**	**3.6045**	**0.7741**
Hoop	Gaussian disc	4,991.77	4,991.77	0.00%	0	0	1

References: Kale et al. (2021) for the solid disc, Garcia et al. (2025) for the tapered web, Eraslan & Orcan (2002) for the Gaussian disc.

The +1.96% hoop-stress figure for the tapered web looks reassuring, but it is not. From 5 to 140 mm our curve runs below the reference by up to 2.08 MPa; beyond about 143 mm it swings above, ending 11.92 MPa higher at R = 200 mm (Figure 8a). The two errors largely cancel in the area, which is why ΔAUC stays small while R^2 falls to 0.774 (bold entries in Table 3). The cause lies in the reference. Garcia et al. (2025) reach their closed-form stress function by dropping the term (r/t)(dt/dr) from the equilibrium equation, which is acceptable only for a gentle taper. For the present 2:1 taper this term equals Br/(A + Br): −0.14 at R = 50 mm, −0.33 at 100 mm, −0.60 at 150 mm, and −1 at the rim, where it is as large as the terms that were kept (Figure 8b). The hoop stress suffers most because, in that formulation, σ_θ is obtained from the derivative of the stress function, so an error in the function's slope passes straight into σ_θ, whereas σ_r comes from the function itself and is pinned to zero at the free rim. Restoring the term turns the reference equation back into the full Eq. (1), which is what our model solves. The independent FEA, which makes no thin-disc approximation, confirms this: its rim hoop stress is 12.85 MPa, against 12.77 MPa from our model and 0.86 MPa from the reference.

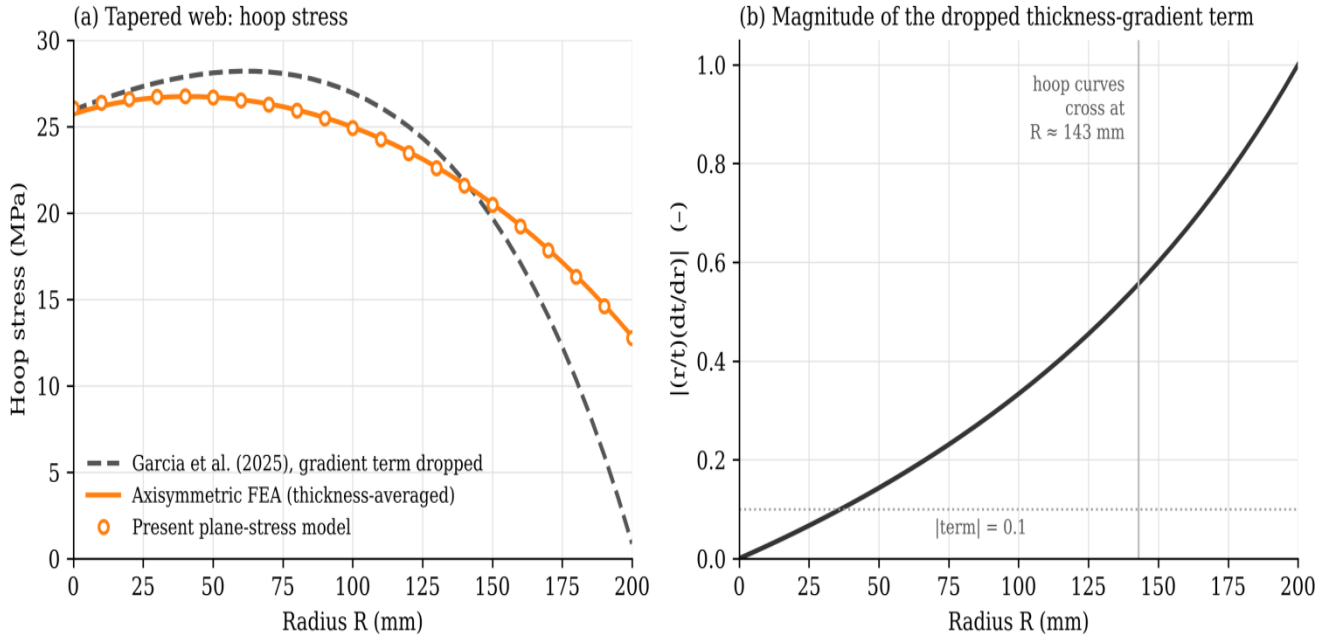


Figure 8. Tapered web: (a) hoop stress from the conical-disc reference, the axisymmetric FEA, and the present model; (b) magnitude of the thickness-gradient term neglected in the reference

ISSN No. 2321-2705 | DOI: 10.51244/IJRSI |Volume XIII Issue X October 2026

Paired t-test

Table 4 lists the t-test outcomes. For the solid disc the mean differences are −0.0431 MPa (radial, p = 0.0170) and +0.1160 MPa (hoop, p < 0.0001). Both reject H_0 at α = 0.05, and the hoop result survives the Bonferroni correction as well. The tapered web gives a clear rejection for radial stress (p < 0.0001) but not for hoop stress (p = 0.3139); there the 95% interval runs from −0.5710 to +1.7334 MPa and includes zero. The Gaussian disc cannot be tested at all. Its differences are zero to four decimals, so $s_d = 0$ and the t-ratio becomes 0/0. Figures 5 and 6 give the full output for the two hoop-stress cases that expose the test's behaviour most clearly.

Table 4. Paired t-test and supporting tests (d = current − reference, N = 40, df = 39)

Stress	Design	Mean d (MPa)	SE (MPa)	95% CI (MPa)	t-ratio	p (two-tailed)	α = 0.05	α = 0.0083	Shapiro–Wilk p	Wilcoxon p
Radial	Solid disc	−0.0431	0.0173	[−0.0781, −0.0082]	−2.494	0.017	Reject	Not reject	0.0016	0.0083
Radial	Tapered web	−0.9666	0.0854	[−1.1394, −0.7938]	−11.316	<0.0001	Reject	Reject	0.0032	6.1×10^{-8}
Radial	Gaussian disc	0	0	–	undefined	–	Not testable	Not testable	–	–
Hoop	Solid disc	0.116	0.0043	[+0.1074, +0.1246]	27.2	<0.0001	Reject	Reject	0.258	3.6×10^{-8}
Hoop	Tapered web	0.5812	0.5696	[−0.5710, +1.7334]	1.02	0.3139	Not reject	Not reject	2.6×10^{-7}	0.444
Hoop	Gaussian disc	0	0	–	undefined	–	Not testable	Not testable	–	–

"Reject" and "Not reject" refer to H_0: $\mu_d = 0$. Bonferroni-adjusted α = 0.05/6 = 0.0083.

ISSN No. 2321-2705 | DOI: 10.51244/IJRSI |Volume XIII Issue X October 2026

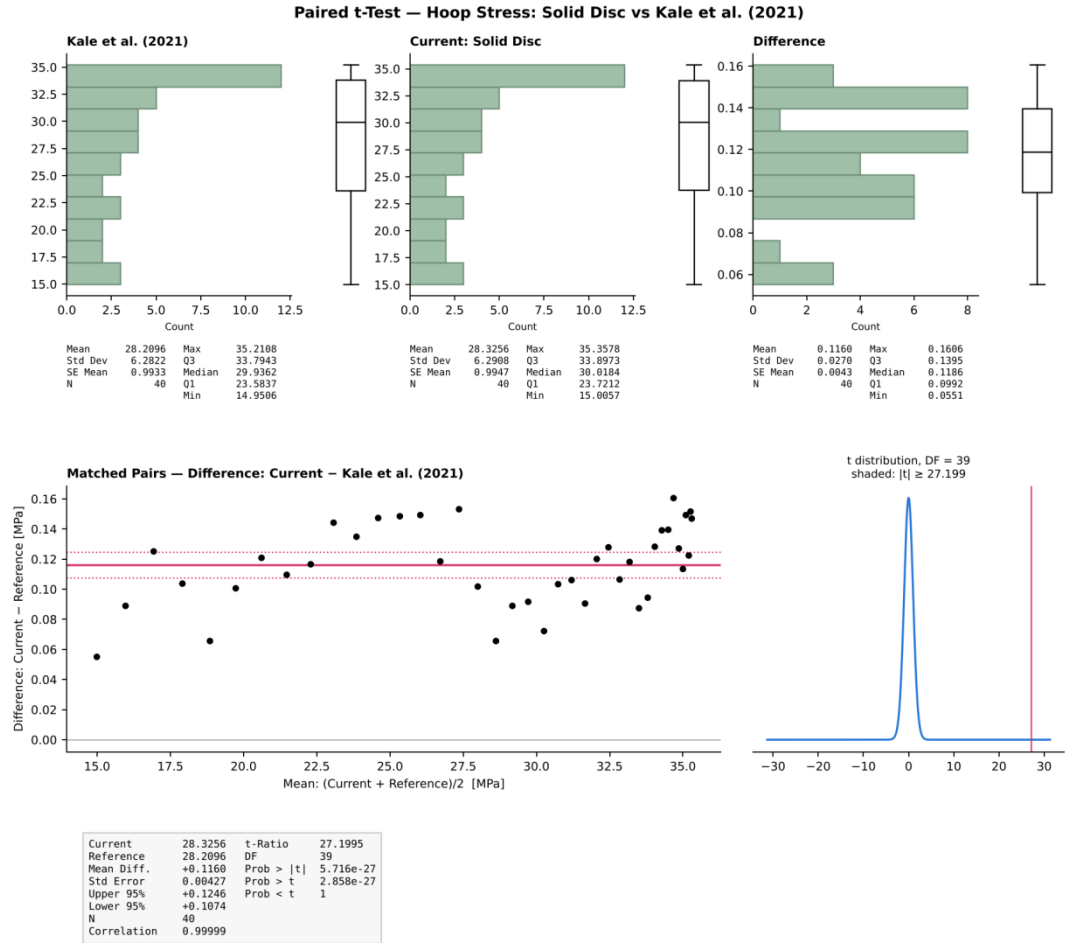


Figure 5. Distributions, matched-pairs plot, t-distribution, and test output for hoop stress, solid disc against Kale et al. (2021)

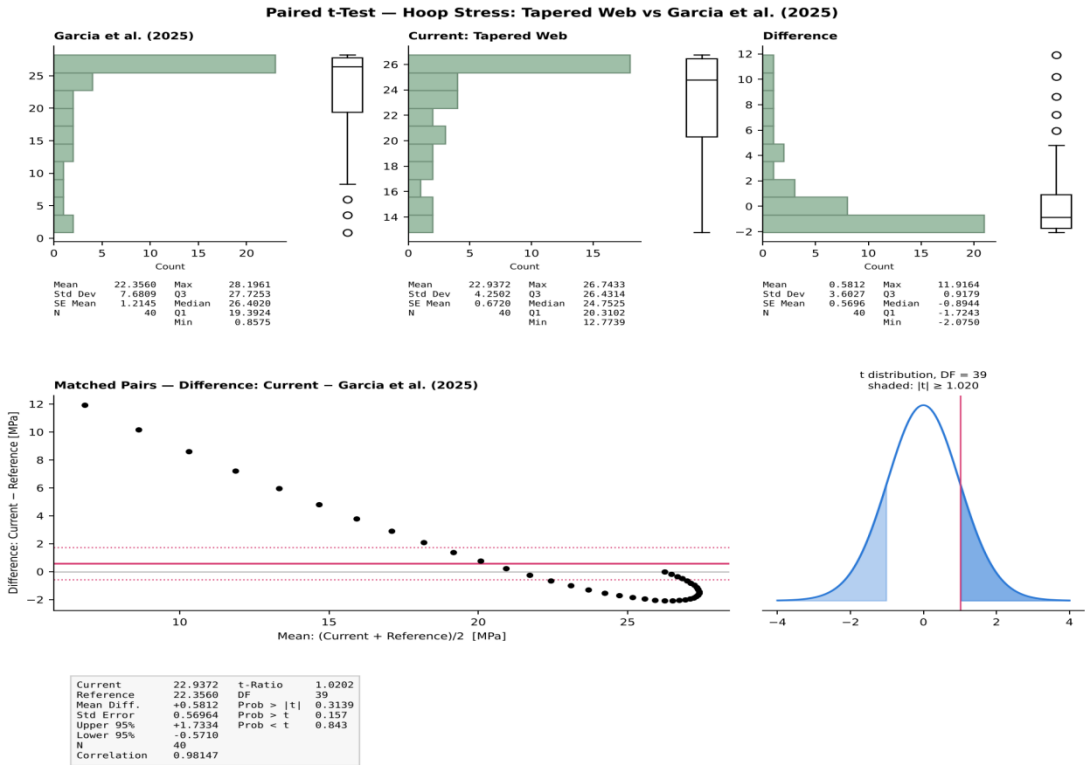


Figure 6. Distributions, matched-pairs plot, t-distribution, and test output for hoop stress, tapered web against Garcia et al. (2025)

ISSN No. 2321-2705 | DOI: 10.51244/IJRSI |Volume XIII Issue X October 2026

Why the t-test disagrees with the AUC

Read literally, the t-test reverses the AUC verdicts. The best-matched model, the solid disc at under 0.5% area error, is declared different. The worst-matched curve, the tapered-web hoop stress with its 11.92 MPa rim error, is not. Nothing is wrong with the arithmetic. The t-ratio divides the mean difference by its own scatter, so it rewards noisy disagreement and punishes steady agreement.

In the solid disc the offsets are minute, 0.04 to 0.12 MPa, which is under half a percent of the stress, but they barely vary along the radius. The standard error of the hoop differences is just 0.0043 MPa, so even this negligible bias pushes t up to 27.2. Figure 5 shows the result: a thin, almost flat band of points near +0.12 MPa. The tapered-web hoop case behaves in the opposite way. The large rim error inflates s_d to 3.60 MPa, the confidence interval widens until it reaches across zero, and the test reports “no difference” (Figure 6). That verdict reflects imprecision, not agreement. The matched-pairs plot makes this plain, because the differences climb steadily with stress level instead of scattering at random, the usual sign that model and reference disagree in a systematic way.

The test's assumptions also fail here. The 40 values are consecutive points on one smooth curve, so neighbouring differences are correlated rather than independent, with lag-1 autocorrelations of 0.50 to 0.89 (Table 5). They are not normal either: Shapiro–Wilk rejects normality in three of the four cases that can be tested (Table 4). Swapping in the Wilcoxon signed-rank test, which needs no normality, changes none of the four decisions. The problem, then, is not only the distribution of the data; it is that the t-test asks a question that validation does not need answered.

Equivalence testing

Table 5 and Figure 7 show the TOST results. Without any correction, the solid disc is equivalent to Kale et al. (2021) for both components, with 90% intervals of −0.072 to −0.014 MPa and +0.109 to +0.123 MPa well inside margins of ±1.16 and ±1.41 MPa. The differences are, however, strongly correlated along the radius, so the effective sample is only 4.3 to 13.4 points rather than 40. Widening the intervals accordingly changes no verdict. The corrected solid-disc intervals, [−0.164, +0.077] and [+0.103, +0.129] MPa, stay inside the margins, the block bootstrap gives similar results, and the largest point-wise difference, 0.22 MPa, is under a fifth of the margin. The Gaussian disc matches Eraslan and Orcan (2002) exactly. The tapered web is not equivalent to Garcia et al. (2025) for either component under any of the three intervals, and its point-wise errors of 1.61 MPa (radial) and 11.92 MPa (hoop) exceed the margins outright. The verdicts are therefore not an artefact of treating the 40 points as independent; the correction would matter mainly in borderline cases, which do not arise here.

Table 5. Equivalence test (TOST, margin ±5% of the reference mean) with and without correction for serial correlation

Stress	Design	Margin Δ_E (MPa)	r_1	N_{eff}	90% CI, N = 40 (MPa)	90% CI, N_{eff} (MPa)	90% CI, block bootstrap (MPa)	max|d| (MPa)	Verdict
Radial	Solid disc	±1.159	0.81	4.3	[−0.072, −0.014]	[−0.164, +0.077]	[−0.109, +0.028]	0.216	Equivalent
Radial	Tapered web	±1.017	0.89	2.2	[−1.111, −0.823]	[−2.672, +0.739]	[−1.398, −0.791]	1.607	Not equivalent
Radial	Gaussian disc	±1.027	–	–	[0, 0]	[0, 0]	[0, 0]	0	Equivalent (identical)
Hoop	Solid disc	±1.410	0.5	13.4	[+0.109, +0.123]	[+0.103, +0.129]	[+0.106, +0.127]	0.161	Equivalent
Hoop	Tapered web	±1.118	0.86	3.1	[−0.379, +1.541]	[−5.318, +6.481]	[−1.583, +1.751]	11.916	Not equivalent
Hoop	Gaussian disc	±1.277	–	–	[0, 0]	[0, 0]	[0, 0]	0	Equivalent (identical)

ISSN No. 2321-2705 | DOI: 10.51244/IJRSI |Volume XIII Issue X October 2026

Verdict requires the N_{eff}-corrected interval, the bootstrap interval, and max|d| all to lie within $\pm\Delta_E$. $N_{eff} = N(1 - r_1)/(1 + r_1)$; bootstrap with blocks of 8 points and 20,000 resamples. Gaussian-disc differences are zero to four decimals, so r_1 and N_{eff} are undefined.

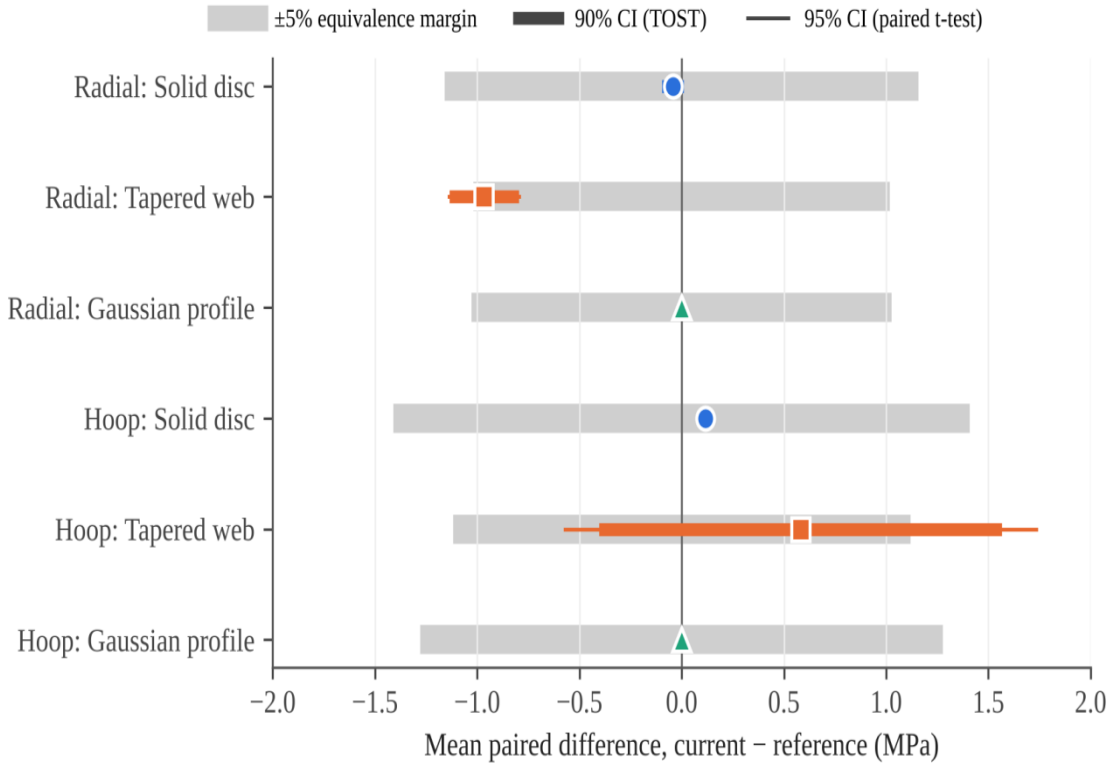


Figure 7. Mean paired differences with 95% (thin) and 90% (thick) confidence intervals, uncorrected for serial correlation, against the ±5% equivalence margins

TOST agrees with the AUC and the point-wise errors, and it overturns both misleading t-test results. The solid disc goes from "significantly different" to "equivalent"; the tapered-web hoop stress goes from "not different" to "not equivalent". The tapered-web radial stress shows why the AUC cannot stand alone either. Its −4.83% passes the 15% limit easily, yet the mean offset of −0.97 MPa is close to 5% of the mean stress, and the 90% interval slips past the margin.

The choice of a 5% margin is a judgement, so we checked how much it matters. The solid-disc verdicts would hold even at ±1% (margins of ±0.23 and ±0.28 MPa): both corrected 90% intervals stay within ±0.17 MPa of zero, and the envelope check passes down to margins of 0.93% (radial) and 0.57% (hoop). The tapered web would need margins of about 5.5% and 6.9% to pass the uncorrected TOST, and 7.9% and 53% to pass the envelope check. The conclusions are therefore not an artefact of where the line was drawn. A tighter margin may be warranted when the stresses feed high-cycle fatigue-life estimates, in which life is much more sensitive to stress than crack-growth rate is; the solid and Gaussian models would still qualify.

Independent finite element verification

Table 7 and Figure 9 compare each model with the axisymmetric FEA. The solid and Gaussian models agree with it to within 0.007 and 0.014 MPa, or 0.02% and 0.04% of peak stress. The tapered web shows the largest difference, 0.32 MPa (1.2% of peak), near the hub, where the 50 mm section is thick enough relative to the radius for out-of-plane effects to matter slightly; beyond R = 50 mm the difference is under 0.12 MPa. All six comparisons pass the envelope check against the FEA by a wide margin. The published references fare differently. Kale et al. (2021) differs from the FEA by no more than 0.22 MPa, but the tapered-web reference differs by up to 12.0 MPa in hoop stress (45% of peak, $R^2 = 0.24$) and 1.64 MPa in radial stress. The FEA therefore places the tapered-web discrepancy in the reference rather than in the model.

ISSN No. 2321-2705 | DOI: 10.51244/IJRSI |Volume XIII Issue X October 2026

Table 7. Independent verification: present models and published references against the axisymmetric FEA

Stress	Design	Model: max|d| (MPa)	Model: % of peak	Model: ΔAUC	Reference: max|d| (MPa)	Reference: % of peak	Reference: R^2
Radial	Solid disc	0	0.00%	0.00%	0.216	0.61%	0.9999
Radial	Tapered web	0.317	1.19%	0.40%	1.637	6.13%	0.9794
Radial	Gaussian disc	0.008	0.02%	0.02%	0.008	0.02%	1
Hoop	Solid disc	0.007	0.02%	0.00%	0.161	0.45%	0.9996
Hoop	Tapered web	0.275	1.03%	−0.09%	11.996	44.88%	0.2385
Hoop	Gaussian disc	0.014	0.04%	0.00%	0.014	0.04%	1

d = model (or reference) − FEA at R = 5–200 mm; FEA mesh 160 × 16 nine-node elements. References as in Table 3.

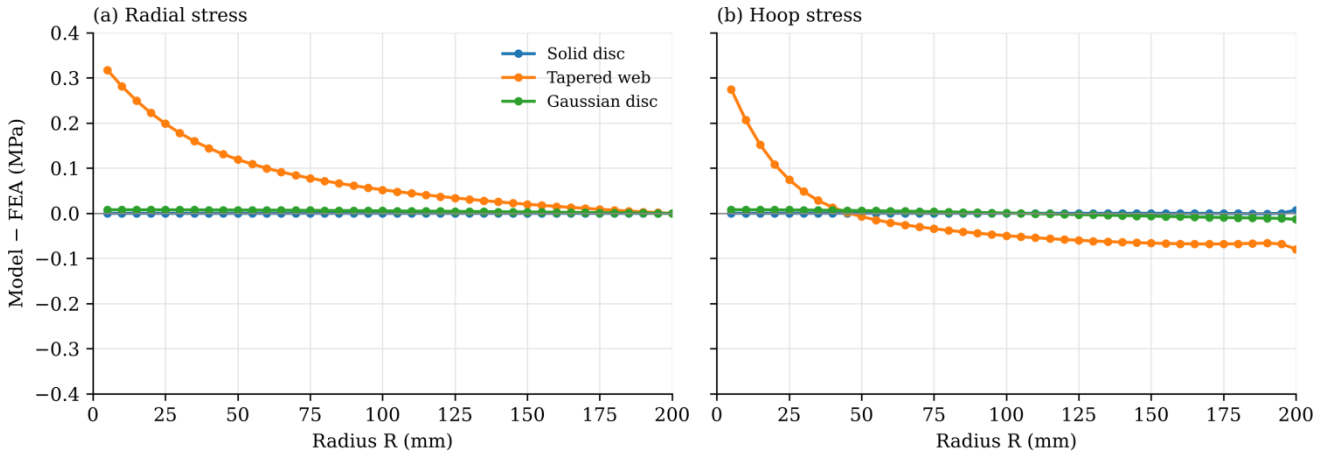


Figure 9. Difference between the present plane-stress models and the axisymmetric FEA: (a) radial and (b) hoop stress

The FEA also supplies the independent check that the Gaussian comparison lacked. The model and its reference agree exactly because they solve the same governing equation, which verifies the solver but cannot show that the equation is adequate. The FEA solves a different set of equations on a different discretisation and still agrees to within 0.04%, which supports the model itself.

Practical implications

The results separate two questions that validation studies often merge. Agreement with a reference was shown for the solid and Gaussian discs and not for the tapered web. Model accuracy, judged against an independent FEA, was shown for all three, the tapered web included, to within 1.2% of peak stress. A model can therefore fail an equivalence test because its reference is inaccurate, and a failed test should prompt a check of the reference before the model is rejected. Three practices follow for anyone applying the procedure: report ΔAUC only together with max|d|, RMSE, and R^2; fix the equivalence margin in advance from the intended use of the stresses; and either correct the test for serial correlation or rely on the point-wise envelope check, which needs no statistical assumptions. For the wider study, the three stress fields can now be carried forward to locate likely crack sites and supply stress amplitudes; what they imply for fatigue life is a question for that stage.

The work has limits. No physical measurements were made; the FEA is an independent numerical check, and

spin-test strain measurements would be the natural next step. The models are axisymmetric, so the three-dimensional stress raisers at a shaft–hub joint, bore, or fillet are not represented, and the discs are solid, linear elastic, isothermal, and loaded only by steady rotation. All comparisons use one common speed set by the benchmark. Finally, the effective-sample-size correction assumes first-order autoregressive dependence, which only approximates smooth deterministic differences; the envelope check is offered for that reason.

CONCLUSION

We built centrifugal stress models of a solid structural-steel disc, a carbon-steel tapered web, and a cast-iron Gaussian disc, compared them with matching reference solutions at 522.57 rad/s, and checked them against an independent axisymmetric FEA. The main findings are as follows.

(i) All six comparisons met the 15% AUC criterion, and also a 5% criterion, yet AUC alone could not detect an 11.92 MPa rim error.

(ii) The paired t-test erred in both directions. It rejected the solid disc, whose mean offsets were only −0.04 and +0.12 MPa, and accepted the tapered-web hoop stress despite an 11.92 MPa rim error and $R^2 = 0.774$, because it scales the mean difference by its scatter. Its independence and normality assumptions were also not met.

(iii) Equivalence testing (TOST, ±5% of the reference mean), corrected for serial correlation and backed by a point-wise envelope check, found the solid and Gaussian discs equivalent to their references and the tapered web not equivalent. The verdicts held for margins from 1% to 5%.

(iv) The FEA agreed with all three models to within 1.2% of peak stress but differed from the conical-disc reference by up to 12.0 MPa, tracing the tapered-web discrepancy to the thickness-gradient term that the reference neglects. The tapered-web model is accurate; its reference is not, near the rim.

(v) In the same steel, the Gaussian disc and tapered web lowered peak stress by 7.0% and 24.0% for 10% and 33% more mass, and at equal peak stress the tapered web stored the most energy per kilogram ($K = 0.718$, against 0.631 and 0.606).

(vi)Validation of deterministic stress models should pair AUC with point-wise errors and a correlation-aware equivalence test against a margin justified by intended use, and should report agreement with a reference separately from model accuracy.

Next, the stress fields will be carried into three-dimensional FEA of the three discs to estimate fatigue life, mixed-mode stress intensity factors, and Paris-law crack growth.

ACKNOWLEDGEMENTS

The first author thanks the Department of Science and Technology – Science and Technology Regional Alliance of Universities for National Development (DOST-STRAND) for funding his graduate studies, and the Graduate School and College of Engineering of Cebu Technological University – Main Campus for academic and computing support. We are grateful to Dr. Gregorio P. Pajaron, Jr., Dr. Jonathan C. Maglasang, Dr. Joecyn N. Archival, and Dr. Ronald M. Galindo for their comments on the work.

ETHICAL CONSIDERATIONS

This study is entirely computational and analytical. It involved no human participants, human data, or animals; ethical approval was therefore not required.

CONFLICT OF INTEREST

The authors have no conflict of interest to declare.

DATA AVAILABILITY

Appendix A lists every radial and hoop stress value used in the validation, including the FEA results (Table A3). The plane-stress and finite element codes and any further data can be obtained from the corresponding author on reasonable request.

REFERENCES

1. Alshoaibi, A. M., & Fageehi, Y. A. (2024). Advances in finite element modeling of fatigue crack propagation. *Applied Sciences, 14*(20), 9297. https://doi.org/10.3390/app14209297
2. American Society of Mechanical Engineers. (2019). *Standard for verification and validation in computational solid mechanics* (ASME V&V 10-2019). ASME.
3. Anderson, T. L. (2017). *Fracture mechanics: Fundamentals and applications* (4th ed.). CRC Press. https://doi.org/10.1201/9781315370293
4. Arun, S., Cole, M. O. T., Chamroon, C., & Fakkaew, W. (2026). Geometry-parametrized stress solution for the rotating conical disk with application to rotor design optimization. *International Journal of Applied Mechanics*. Advance online publication. https://doi.org/10.1142/S1758825126500249
5. Bayley, G. V., & Hammersley, J. M. (1946). The "effective" number of independent observations in an autocorrelated time series. *Supplement to the Journal of the Royal Statistical Society, 8*(2), 184–197. https://doi.org/10.2307/2983560
6. Berger, M., & Porat, I. (1988). Optimal design of a rotating disk for kinetic energy storage. *Journal of Applied Mechanics, 55*(1), 164–170. https://doi.org/10.1115/1.3173623
7. Bland, J. M., & Altman, D. G. (1986). Statistical methods for assessing agreement between two methods of clinical measurement. *The Lancet, 327*(8476), 307–310. https://doi.org/10.1016/S0140-6736(86)90837-8
8. Coppedé, D., Bortoli, F. da S., de Moura, A. C. G., Moreira, J. M. L., & Frajuca, C. (2024). Study of geometries and stability for energy density in electromechanical battery flywheels with a Gaussian shape. *Journal of Physics: Conference Series, 2701*(1), 012060. https://doi.org/10.1088/1742-6596/2701/1/012060
9. Dunn, O. J. (1961). Multiple comparisons among means. *Journal of the American Statistical Association, 56*(293), 52–64. https://doi.org/10.1080/01621459.1961.10482090
10. Eraslan, A. N. (2005). A class of nonisothermal variable thickness rotating disk problems solved by hypergeometric functions. *Turkish Journal of Engineering and Environmental Sciences, 29*, 241–269.
11. Eraslan, A. N., & Orcan, Y. (2002). Elastic–plastic deformation of a rotating solid disk of exponentially varying thickness. *Mechanics of Materials, 34*(7), 423–432. https://doi.org/10.1016/S0167-6636(02)00117-5
12. Garcia, M., Orozco-López, O., Uribe-Chavira, J., & Blanco-Ortega, A. (2025). An analytical approximation of the stress function for conical flywheels. *Applied Mechanics, 6*(2), 30. https://doi.org/10.3390/applmech6020030
13. Kale, V., & Secanell, M. (2018). A comparative study between optimal metal and composite rotors for flywheel energy storage systems. *Energy Reports, 4*, 576–585. https://doi.org/10.1016/j.egyr.2018.09.003
14. Kale, V., Thomas, M., & Secanell, M. (2021). On determining the optimal shape, speed, and size of metal flywheel rotors with maximum kinetic energy. *Structural and Multidisciplinary Optimization, 64*(3), 1481–1499. https://doi.org/10.1007/s00158-021-02935-x
15. Künsch, H. R. (1989). The jackknife and the bootstrap for general stationary observations. *The Annals of Statistics, 17*(3), 1217–1241. https://doi.org/10.1214/aos/1176347265
16. Lakens, D. (2017). Equivalence tests: A practical primer for t tests, correlations, and meta-analyses. *Social Psychological and Personality Science, 8*(4), 355–362. https://doi.org/10.1177/1948550617697177
17. Li, X., & Palazzolo, A. (2022). A review of flywheel energy storage systems: State of the art and opportunities. *Journal of Energy Storage, 46*, 103576. https://doi.org/10.1016/j.est.2021.103576

18. Nuñez, A. B., Ubando, A. T., Gonzaga, J. A., Navea, R. F. R., Santos, G. N. C., & Chen, W.-H. (2025). Crack propagation in an energy storage flywheel rotor using finite element method. *Results in Engineering, 27*, 105842. https://doi.org/10.1016/j.rineng.2025.105842
19. Oberkampf, W. L., & Roy, C. J. (2010). *Verification and validation in scientific computing*. Cambridge University Press. https://doi.org/10.1017/CBO9780511760396
20. Paris, P. C., Gomez, M. P., & Anderson, W. E. (1961). A rational analytic theory of fatigue. *The Trend in Engineering, 13*, 9–14.
21. Pullen, K. R. (2019). The status and future of flywheel energy storage. *Joule, 3*(6), 1394–1399. https://doi.org/10.1016/j.joule.2019.04.006
22. Rouse, J. P., Garvey, S. D., Cárdenas, B., Hoskin, A., Swinfen-Styles, L., & Xu, W. (2021). A case study investigation into the risk of fatigue in synchronous flywheel energy stores and ramifications for the design of inertia replacement systems. *Journal of Energy Storage, 39*, 102651. https://doi.org/10.1016/j.est.2021.102651
23. Schuirmann, D. J. (1987). A comparison of the two one-sided tests procedure and the power approach for assessing the equivalence of average bioavailability. *Journal of Pharmacokinetics and Biopharmaceutics, 15*(6), 657–680. https://doi.org/10.1007/BF01068419
24. Shapiro, S. S., & Wilk, M. B. (1965). An analysis of variance test for normality (complete samples). *Biometrika, 52*(3–4), 591–611. https://doi.org/10.1093/biomet/52.3-4.591
25. Stodola, A. (1927). *Steam and gas turbines* (L. C. Loewenstein, Trans.; Vol. 1). McGraw-Hill.
26. Timoshenko, S. P., & Goodier, J. N. (1970). *Theory of elasticity* (3rd ed.). McGraw-Hill.
27. Wang, L., Shatil, G., & Ren, X. (2002). Assessment of fatigue and fracture strength of transportation energy storage flywheel using finite element simulation. *WIT Transactions on Engineering Sciences, 37*. https://doi.org/10.2495/DM020231
28. Wilcoxon, F. (1945). Individual comparisons by ranking methods. *Biometrics Bulletin, 1*(6), 80–83. https://doi.org/10.2307/3001968
29. Xu, K., Guo, Y., Lei, G., & Zhu, J. (2023). A review of flywheel energy storage system technologies. *Energies, 16*(18), 6462. https://doi.org/10.3390/en16186462

APPENDIX A. POINT-WISE VALIDATION DATA

All stresses are in MPa at ω = 522.57 rad/s and b = 0.2 m; d = current model − reference. Kale et al. (2021) report no value at R = 0 mm, which was therefore excluded from all statistics. Table A3 gives the thickness-averaged stresses from the axisymmetric FEA (160 × 16 nine-node elements).

Table A1. Radial stress distribution: present models versus reference studies (MPa)

R (mm)	Kale et al.	Solid disc	d	Garcia et al.	Tapered web	d	Eraslan & Orcan	Gaussian	d
0	–	35.3706	–	25.9384	26.0705	0.1321	30.8866	30.8866	0
5	35.2464	35.3485	0.1021	26.2445	26.3011	0.0566	30.8689	30.8689	0
10	35.2518	35.2821	0.0303	26.514	26.4932	−0.0208	30.8156	30.8156	0
15	35.1203	35.1716	0.0513	26.7464	26.6465	−0.0999	30.7267	30.7267	0
20	34.9114	35.0169	0.1055	26.9412	26.7607	−0.1805	30.6023	30.6023	0
25	34.7134	34.8179	0.1045	27.0978	26.8355	−0.2623	30.4422	30.4422	0
30	34.4488	34.5747	0.1259	27.2156	26.8706	−0.3450	30.2462	30.2462	0
35	34.1821	34.2873	0.1052	27.294	26.8655	−0.4285	30.0144	30.0144	0
40	33.9184	33.9557	0.0373	27.3323	26.82	−0.5123	29.7465	29.7465	0
45	33.4503	33.5799	0.1296	27.3298	26.7338	−0.5960	29.4425	29.4425	0
50	33.1168	33.1599	0.0431	27.2859	26.6062	−0.6797	29.102	29.102	0
55	32.5764	32.6957	0.1193	27.1996	26.4371	−0.7625	28.7248	28.7248	0
60	32.1168	32.1872	0.0704	27.0703	26.2258	−0.8445	28.3109	28.3109	0
65	31.5847	31.6345	0.0498	26.8969	25.972	−0.9249	27.8598	27.8598	0

ISSN No. 2321-2705 | DOI: 10.51244/IJRSI |Volume XIII Issue X October 2026

70	30.9825	31.0377	0.0552	26.6787	25.6751	−1.0036	27.3713	27.3713	0
75	30.3075	30.3966	0.0891	26.4146	25.3346	−1.0800	26.8451	26.8451	0
80	29.6473	29.7113	0.064	26.1035	24.9499	−1.1536	26.2809	26.2809	0
85	29.078	28.9818	−0.0962	25.7443	24.5205	−1.2238	25.6783	25.6783	0
90	28.3204	28.208	−0.1124	25.336	24.0456	−1.2904	25.037	25.037	0
95	27.5134	27.3901	−0.1233	24.8771	23.5246	−1.3525	24.3565	24.3565	0
100	26.5685	26.5279	−0.0406	24.3664	22.9568	−1.4096	23.6363	23.6363	0
105	25.7569	25.6215	−0.1354	23.8024	22.3414	−1.4610	22.8761	22.8761	0
110	24.7564	24.671	−0.0854	23.1836	21.6775	−1.5061	22.0754	22.0754	0
115	23.7843	23.6762	−0.1081	22.5083	20.9643	−1.5440	21.2336	21.2336	0
120	22.7114	22.6372	−0.0742	21.7748	20.2008	−1.5740	20.3503	20.3503	0
125	21.6529	21.5539	−0.0990	20.9812	19.386	−1.5952	19.4247	19.4247	0
130	20.5098	20.4265	−0.0833	20.1254	18.5188	−1.6066	18.4564	18.4564	0
135	19.3285	19.2548	−0.0737	19.2053	17.5979	−1.6074	17.4448	17.4448	0
140	18.1893	18.039	−0.1503	18.2186	16.6223	−1.5963	16.389	16.389	0
145	16.8412	16.7789	−0.0623	17.1626	15.5903	−1.5723	15.2886	15.2886	0
150	15.6364	15.4746	−0.1618	16.0347	14.5007	−1.5340	14.1427	14.1427	0
155	14.2849	14.1261	−0.1588	14.8318	13.3518	−1.4800	12.9505	12.9505	0
160	12.8685	12.7334	−0.1351	13.5509	12.1418	−1.4091	11.7114	11.7114	0
165	11.4545	11.2965	−0.1580	12.1883	10.8689	−1.3194	10.4245	10.4245	0
170	9.9792	9.8153	−0.1639	10.7403	9.5311	−1.2092	9.0888	9.0888	0
175	8.4131	8.29	−0.1231	9.2029	8.126	−1.0769	7.7036	7.7036	0
180	6.8691	6.7204	−0.1487	7.5714	6.6514	−0.9200	6.2679	6.2679	0
185	5.2659	5.1066	−0.1593	5.8411	5.1045	−0.7366	4.7807	4.7807	0
190	3.6548	3.4486	−0.2062	4.0064	3.4825	−0.5239	3.2411	3.2411	0
195	1.8791	1.7464	−0.1327	2.0616	1.7822	−0.2794	1.6478	1.6478	0
200	0.2159	0	−0.2159	0	0	0	0	0	0

Table A2. Hoop stress distribution: present models versus reference studies (MPa)

R (mm)	Kale et al.	Solid disc	d	Garcia et al.	Tapered web	d	Eraslan & Orcan	Gaussian	d
0	–	35.3706	–	25.9384	26.0705	0.1321	30.8866	30.8866	0
5	35.2108	35.3578	0.147	26.2538	26.2332	−0.0206	30.8773	30.8773	0
10	35.1678	35.3196	0.1518	26.5506	26.3738	−0.1768	30.8494	30.8494	0
15	35.1333	35.256	0.1227	26.8277	26.4921	−0.3356	30.803	30.803	0
20	35.0175	35.1669	0.1494	27.0838	26.5879	−0.4959	30.7379	30.7379	0
25	34.9389	35.0524	0.1135	27.3175	26.6611	−0.6564	30.6541	30.6541	0
30	34.7852	34.9123	0.1271	27.5274	26.7115	−0.8159	30.5517	30.5517	0
35	34.5863	34.7469	0.1606	27.712	26.739	−0.9730	30.4305	30.4305	0
40	34.4164	34.556	0.1396	27.8696	26.7433	−1.1263	30.2905	30.2905	0
45	34.2001	34.3396	0.1395	27.9987	26.7244	−1.2743	30.1317	30.1317	0
50	33.9695	34.0978	0.1283	28.0974	26.6819	−1.4155	29.9539	29.9539	0
55	33.7359	33.8305	0.0946	28.1638	26.6157	−1.5481	29.757	29.757	0
60	33.4503	33.5377	0.0874	28.1961	26.5255	−1.6706	29.5411	29.5411	0
65	33.1013	33.2195	0.1183	28.192	26.4112	−1.7808	29.3059	29.3059	0
70	32.7693	32.8759	0.1066	28.1492	26.2724	−1.8768	29.0513	29.0513	0

75	32.3787	32.5067	0.128	28.0656	26.109	−1.9566	28.7773	28.7773	0
80	31.9921	32.1122	0.1201	27.9385	25.9206	−2.0179	28.4836	28.4836	0
85	31.6014	31.6922	0.0908	27.7652	25.707	−2.0582	28.1702	28.1702	0
90	31.1405	31.2467	0.1062	27.5428	25.4678	−2.0750	27.8369	27.8369	0
95	30.6723	30.7757	0.1034	27.2685	25.2028	−2.0657	27.4835	27.4835	0
100	30.2069	30.2793	0.0724	26.9388	24.9115	−2.0273	27.1099	27.1099	0
105	29.6655	29.7575	0.092	26.5503	24.5936	−1.9567	26.7158	26.7158	0
110	29.1209	29.2102	0.0893	26.0994	24.2488	−1.8506	26.301	26.301	0
115	28.5718	28.6374	0.0656	25.582	23.8766	−1.7054	25.8655	25.8655	0
120	27.9372	28.0392	0.102	24.994	23.4765	−1.5175	25.4088	25.4088	0
125	27.2622	27.4155	0.1533	24.3307	23.0482	−1.2825	24.9309	24.9309	0
130	26.6475	26.7664	0.1188	23.5872	22.591	−0.9962	24.4314	24.4314	0
135	25.9424	26.0918	0.1494	22.7583	22.1045	−0.6538	23.9101	23.9101	0
140	25.2432	25.3918	0.1486	21.8384	21.588	−0.2504	23.3668	23.3668	0
145	24.5188	24.6663	0.1475	20.8213	21.041	0.2197	22.8011	22.8011	0
150	23.7801	23.9153	0.1352	19.7003	20.4628	0.7625	22.2128	22.2128	0
155	22.9945	23.1389	0.1444	18.4685	19.8526	1.3841	21.6016	21.6016	0
160	22.2201	22.337	0.1169	17.1179	19.2098	2.0919	20.9671	20.9671	0
165	21.3999	21.5097	0.1098	15.6403	18.5334	2.8931	20.309	20.309	0
170	20.5359	20.6569	0.121	14.0265	17.8226	3.7961	19.627	19.627	0
175	19.678	19.7787	0.1007	12.2666	17.0764	4.8098	18.9207	18.9207	0
180	18.8094	18.875	0.0656	10.3496	16.2937	5.9441	18.1897	18.1897	0
185	17.842	17.9459	0.1039	8.2639	15.4734	7.2095	17.4337	17.4337	0
190	16.866	16.9913	0.1253	5.9964	14.6143	8.6179	16.6522	16.6522	0
195	15.9222	16.0112	0.089	3.5328	13.7149	10.1821	15.8449	15.8449	0
200	14.9506	15.0057	0.0551	0.8575	12.7739	11.9164	15.0112	15.0112	0

Table A3. Thickness-averaged radial and hoop stresses from the axisymmetric FEA (MPa)

R (mm)	Radial: solid disc	Radial: tapered web	Radial: Gaussian disc	Hoop: solid disc	Hoop: tapered web	Hoop: Gaussian disc
0	35.371	25.7161	30.8791	35.371	25.7161	30.8791
5	35.3488	25.9837	30.8612	35.358	25.9585	30.8696
10	35.2824	26.212	30.808	35.3198	26.1672	30.8418
15	35.1719	26.3968	30.7192	35.2562	26.3404	30.7954
20	35.0172	26.5385	30.5948	35.1671	26.4797	30.7304
25	34.8182	26.6372	30.4347	35.0525	26.5869	30.6469
30	34.575	26.6929	30.2388	34.9125	26.6634	30.5447
35	34.2876	26.7057	30.0071	34.747	26.7108	30.4237
40	33.956	26.6758	29.7393	34.5561	26.7303	30.2841
45	33.5802	26.6029	29.4353	34.3397	26.7229	30.1256
50	33.1602	26.4872	29.0949	34.0979	26.6895	29.9481
55	32.696	26.3283	28.7179	33.8306	26.6306	29.7517
60	32.1875	26.1262	28.3041	33.5379	26.5464	29.5362
65	31.6348	25.8805	27.8532	33.2197	26.4371	29.3014
70	31.038	25.5909	27.3649	32.876	26.3028	29.0474

ISSN No. 2321-2705 | DOI: 10.51244/IJRSI |Volume XIII Issue X October 2026

75	30.3969	25.257	26.8389	32.5069	26.1434	28.7739
80	29.7116	24.8783	26.2748	32.1123	25.9586	28.4808
85	28.982	24.4544	25.6724	31.6923	25.7482	28.168
90	28.2083	23.9846	25.0313	31.2468	25.5121	27.8353
95	27.3904	23.4683	24.351	30.7759	25.2499	27.4825
100	26.5282	22.9048	23.6311	30.2795	24.9612	27.1095
105	25.6218	22.2935	22.8711	29.7576	24.6458	26.716
110	24.6713	21.6334	22.0706	29.2103	24.3031	26.302
115	23.6765	20.9238	21.2291	28.6376	23.933	25.8671
120	22.6374	20.1638	20.346	28.0394	23.5348	25.4111
125	21.5542	19.3522	19.4207	27.4157	23.1081	24.9339
130	20.4268	18.488	18.4527	26.7665	22.6525	24.4351
135	19.2551	17.5701	17.4412	26.092	22.1674	23.9145
140	18.0393	16.5972	16.3858	25.3919	21.6521	23.3718
145	16.7792	15.5679	15.2856	24.6664	21.1062	22.8068
150	15.4749	14.4808	14.14	23.9155	20.5289	22.2192
155	14.1264	13.3343	12.9481	23.139	19.9195	21.6086
160	12.7337	12.1267	11.7093	22.3372	19.2773	20.9748
165	11.2967	10.856	10.4227	21.5099	18.6013	20.3173
170	9.8156	9.5203	9.0873	20.6572	17.8907	19.6359
175	8.2902	8.1173	7.7024	19.7791	17.1444	18.9302
180	6.7207	6.6446	6.267	18.8757	16.3613	18.1997
185	5.1069	5.0996	4.7801	17.9469	15.5402	17.4441
190	3.4489	3.4794	3.2408	16.9925	14.6805	16.6631
195	1.7467	1.7809	1.6478	16.011	13.783	15.8564
200	0.0002	0.0007	0.0003	14.9987	12.8533	15.0248